doi.org/10.36721/PJPS.2026.39.11.323.1

MicroRNA-135 alleviates cisplatin resistance in cervical cancer by inhibiting CD44v6

Rui Zhou[1,2#], Hongmei Wang[1#], Anji Li[1] and Shuhan Lv[1]*

[1]The First Clinical Medical College of Guizhou University of Traditional Chinese Medicine, Guiyang, Guizhou, 550001, China
[2]Department of Obstetrics and Gynecology, Zunyi Hospital of Traditional Chinese Medicine, Zunyi, Guizhou, 563000, China

Abstract: **Background**: Cervical cancer (CC) remains a leading cause of cancer-related mortality worldwide and cisplatin resistance poses a major challenge to effective treatment. MicroRNA-135 (miR-135) has been implicated in tumor progression and drug resistance, but its role in cisplatin-resistant CC remains unclear. **Objectives**: To investigate whether miR-135 affects cisplatin resistance in CC cells by targeting CD44v6. **Methods**: Bioinformatic analysis (TargetScan) was performed to predict the miR-135 binding site in CD44v6, followed by a dual-luciferase reporter assay. RT-qPCR and Western blot were used to measure miR-135 and CD44v6 expression in cisplatin-resistant HeLa/DDP cells, HeLa cells and normal Ect1/E6E7 cells. HeLa/DDP cells were transfected with miR-135 mimic or NC mimic and cell proliferation (CCK-8, colony formation), apoptosis (flow cytometry) and CD44v6 expression were assessed. **Results**: miR-135 directly bound to the CD44v6 3‘-UTR, reducing luciferase activity by 58% (*p* < 0.001). miR-135 expression was decreased by 68% in HeLa/DDP cells compared to Ect1/E6E7 cells, while CD44v6 expression was increased 3.5-fold. miR-135 mimic transfection reduced CD44v6 protein expression by 62%, decreased cell viability by 57.3%, increased the apoptosis rate from 12.4% to 35.8% (absolute increase of 23.4%) and lowered the cisplatin IC50 from 22.36 to 8.47 μmol/L (2.64-fold reversal, *p* < 0.001). **Conclusions**: miR-135 overexpression was associated with reduced CD44v6 expression, decreased proliferation, increased apoptosis and enhanced sensitivity to cisplatin in HeLa/DDP cells. These findings demonstrate an inverse association between miR-135 and CD44v6 in cisplatin-resistant CC cells; however, causal mechanistic evidence (e.g., via CD44v6-specific knockdown or rescue experiments) is not provided. Further studies are required to establish whether CD44v6 directly mediates the chemosensitizing effects of miR-135.

Keywords: CD44v6; Cervical cancer; Drug resistance; miR-135

Submitted on 02-02-2026 – Revised on 26-05-2026 – Accepted on 04-06-2026

INTRODUCTION

Cervical cancer (CC) is the second leading cause of cancer-related death, with 135,000 annual cases in China (Liu *et al*., 2025). Surgery is the primary treatment option with adjuvant radiotherapy and chemotherapy, but the high-cost regimen results in severe side effects and thus the prognosis remains poor (Zhao *et al*., 2026). Chemotherapy, a commonly used treatment, kills cancer cells to prevent tumor growth but also affects the function of normal cells, leading to adverse reactions and drug resistance (Zhang G *et al*., 2025; Tao *et al*., 2023).

MicroRNAs (miRNAs) are endogenous non-coding RNAs that are aberrantly expressed in multiple solid tumors, including breast, colon and ovarian cancers, where they regulate tumorigenesis, metastasis and chemotherapy resistance (Di Martino *et al*., 2025). Among them, miR-135 has attracted widespread attention due to its aberrant expression in multiple cancer types and its close association with chemotherapy response. Previous reports have shown that miR-135 exhibits both tumor-suppressive and oncogenic roles. It is downregulated in prostate, kidney, gallbladder, and nasopharyngeal cancers, as well as glioma, and is upregulated in bladder, oral, colorectal, and liver cancers, and exhibits dual roles in breast, gastric, lung, pancreatic, and head-and-neck cancers (Kadkhoda *et al*., 2022). In esophageal cancer, cisplatin treatment reduces miR-135b-5p expression and overexpression of miR-135b-5p attenuates the cytotoxic effects of cisplatin (Cataldi-Stagetti *et al*., 2026). In ovarian cancer, miR-135a-3p overexpression enhances sensitivity to cisplatin and paclitaxel (Kadkhoda *et al*., 2022). miR-135 expression increased 39-fold in the early stage of CC. Abnormal expression of miR-135 was detected in CC tissue and was involved in CC development and drug resistance (Feitosa *et al*., 2024; Bencheikh *et al*., 2026). In the present study, bioinformatics analysis indicated that miR-135 might bind to the 3′-UTR of CD44v6, thereby regulating the transcription of tumor-related genes. Similarly, overexpression of miR-135 has been shown to inhibit malignant phenotypes of cancer cells and angiogenesis by targeting CD44 (Zhou *et al*., 2025; Park *et al*., 2025).

In triple-negative breast cancer cells, the induction of migration attenuated the correlation between CD44v and the cytoskeleton, accompanied by increased interaction

**Corresponding author:* e-mail: l13229498004@sina.com
#These authors contributed equally and are the co-first authors.

between CD44v and active Ezrin (a cytoskeletal connector) (Raftery *et al*., 2023). Migration of mesenchymal stem cells induced by VEGF altered the size of the CD44v-mediated cell domain, resulting in FAK activation and cytoskeletal rearrangement (Lee *et al*., 2025). Previous studies have noted that CD44v plays an important role in drug resistance in liver cancer and other tumor cells (Srikanth *et al*., 2025). The six CD44 variants (CD44v6) are involved in tumor development and progression in various ways. In ovarian cancer, CD44v6 is highly expressed on cancer stem cells from distant metastases and correlates with poor prognosis, suggesting its involvement in tumor progression and chemoresistance (Wilczynski *et al*., 2022). However, the role of CD44 variants in cisplatin resistance in CC remains insufficiently characterized. In the current study, miR-135 and CD44v6 levels were evaluated in cisplatin (cis-diamminedichloroplatinum II, DDP)-resistant CC cell lines and parental CC cells. Furthermore, *in-vitro* experiments were conducted to investigate whether miR-135 and CD44v6 expression affected proliferation, apoptosis and drug resistance.

MATERIALS AND METHODS

Reagents and materials

Human normal cervical epithelial cells Ect1/E6E7 and CC HeLa cells were obtained from Dinghaoyuan Biotechnology Co., Ltd. (China); HEK293T cells and HeLa/DDP drug-resistant cells from Shanghai Yisheng Biotechnology Co., Ltd. (China). The reagents and other materials included: RPMI 1640 medium (Chengdu Beisite Reagent Co., Ltd., China), Opti-MEM (Shanghai Zhiji Biochemical Technology Co., Ltd., China), fetal bovine serum (FBS, Fenghui Biocell Line Company, China); Trizol (Qingke Biotechnology Company, China), Lipofectamine 2000 transfection reagent (Shanghai Hanni Cell Biotechnology Co., Ltd., China); PrimeScript RT reagent Kit (Zhejiang Gelusite Biotechnology Company, China); miR-135 mimic and miR-NC (Zhongyuan Xiehe Cell Genetic Engineering Co., Ltd. China); CD44v6 antibody (Beijing Sipaerke Cell Technology Co., Ltd., China); β-actin antibody (Suzhou Ruisitan Cell Bank Co., Ltd., China); secondary antibody (Guangzhou Saiku Biotechnology Co., Ltd., China); CCK-8 detection reagent (Jiuzhitang Maker (Beijing) Cell Technology Co., Ltd. China); Annexin V/PI apoptosis detection reagents (Chengdu Beisite Reagent Co., Ltd., China); BeyoECL Plus and EdU detection reagents (Jiangsu Beyotime Biotechnology, China).

Cell culture

Ect1/E6E7, HeLa and HEK293T cells were cultured in RPMI 1640 medium containing 10% FBS in a humidified incubator at 37°C with 5% CO_2. All cell lines tested negative for mycoplasma.

Establishment and maintenance of cisplatin-resistant cell line

A cisplatin-resistant HeLa/DDP cell line was established using the intermittent concentration gradient induction method. The parental HeLa cells were initially cultured in RPMI 1640 medium (containing 10% FBS) with 0.1 μmol/L cisplatin (DDP). The medium was replaced every 3-4 days. When the cells resumed normal growth at 0.1 μmol/L cisplatin, the concentration was gradually increased to 0.1-0.2 μmol/L, and each concentration was maintained for 2-3 weeks. The entire process lasted approximately 6 months, and a resistant cell line that grew stably in the presence of 2.0 μmol/L cisplatin was finally obtained and designated HeLa/DDP. To maintain the resistant phenotype, the HeLa/DDP cells were routinely cultured in medium containing 1.0 μmol/L cisplatin. Before the experiment, the cells were cultured in cisplatin-free medium for 7 days to eliminate short-term stress effects. Resistance stability verification: The IC50 value in HeLa/DDP cells was measured every 5 generations to confirm that the resistance ratio relative to the parental cells remained stable within the range of 4.5-5.5 times. The cells used in this experiment were the 10th to 20th generation. Resistance index = IC50 (resistant cells) / IC50 (parental cells). Resistance reversal ratio = IC50 (NC mimic group) / IC50 (miR-135 mimic group).

qRT-PCR

Total RNA was extracted from cells using Trizol reagent (Invitrogen, USA). RNA purity was assessed using a NanoDrop 2000 (Thermo Fisher, USA), with A260/A280 ratios between 1.8 and 2.0. Reverse transcription of 1 μg total RNA to cDNA was performed using the PrimeScript RT kit (Takara, Japan) under the following conditions: 37°C for 15 minutes, 85°C for 5 seconds. qRT-PCR was performed using TB Green Premix Ex Taq II (Takara, Japan) on an ABI 7500 Real-Time PCR System (Applied Biosystems, USA). The reaction mixture (20 μL) contained 10 μL TB Green Premix, 0.8 μL each of forward and reverse primers (10 μmol/L) and 2 μL cDNA. The cycling conditions were: 95°C for 30 seconds, followed by 40 cycles of 95°C for 5 seconds and 60°C for 34 seconds. Each sample was tested in triplicate technical replicates. Primer sequences were as follows: CD44v6 forward 5‘-CAGCTATCCCAACCAACACC-3’, reverse 5‘-GGCCTCTGTGTTGTTGTTGG-3’ (product 142 bp, targeting v6 exon). miR-135 was reverse-transcribed using the stem-loop method with primers designed by RiboBio (China). U6 snRNA (internal control for miR-135): forward 5‘-CTCGCTTCGGCAGCACA-3’, reverse 5‘-AACGCTTCACGAATTTGCGT-3’; GAPDH (internal control for CD44v6): forward 5’-GGAGCGAGATCCCTCCAAAAT-3‘, reverse 5’-GGCTGTTGTCATACTTCTCATGG-3‘. Data were analyzed using the 2^(-ΔΔCt) method. miR-135 expression was normalized to U6 and CD44v6 expression was normalized to GAPDH, with the control group set to 1.0.

Cell transfection

Cell preparation: 24 hours before transfection, HeLa or HeLa/DDP cells in the logarithmic growth phase were trypsinized with 0.25% trypsin and seeded into 6-well plates at a density of 2×10^5 cells per well in 2 mL of antibiotic-free RPMI 1640 medium supplemented with 10% FBS. After 24 hours of culture, cells reached 70%-80% confluence for transfection. Transfection reagent and dosage: Lipofectamine 2000 transfection reagent (Invitrogen, USA, catalog No. 11668019) was used. Briefly, 100 pmol of miR-135 mimic or NC mimic (Bioneer, Korea) was diluted in 150 μL Opti-MEM serum-free medium (Gibco, USA). Separately, 5 μL Lipofectamine 2000 was diluted in 150 μL Opti-MEM and incubated at room temperature for 5 minutes. The diluted miRNA and diluted transfection reagent were mixed at a 1:1 ratio, gently pipetted and incubated at room temperature for 20 minutes to form transfection complexes. The transfection complexes (300 μL) were added dropwise to the 6-well plates containing cells and the plates were gently swirled to ensure even distribution. Post-transfection culture: Cells were cultured in a 37°C, 5% CO_2 incubator. Six hours after transfection, the medium was replaced with fresh RPMI 1640 complete medium containing 10% FBS (antibiotic-free). Cells were cultured for an additional 48 hours before being harvested for subsequent experiments (qRT-PCR, Western blot, CCK-8, flow cytometry, etc.). Transfection efficiency validation: FAM-labeled NC mimic was used as a transfection efficiency control in each experiment. 48 hours after transfection, the percentage of green fluorescence-positive cells was assessed under a fluorescence microscope to confirm transfection efficiency ≥80%. Each experiment was performed with triplicate wells and independently repeated three times.

Bioinformatic analysis

The TargetScan database (version 7.2) was used to predict potential target genes of miR-135. Human (Homo sapiens) was selected as the species and the miRNA ID was hsa-miR-135a-5p. The prediction algorithm used the Total context++ score to assess the probability of miRNA binding to the target gene's 3′ UTR, considering factors such as seed-sequence match type, binding-site position, flanking-sequence nucleotide composition and cross-species conservation. The screening threshold was set at context++ score ≤ -0.20 (corresponding to the 80th percentile of prediction reliability). Additionally, the seed sequence (positions 2-8) of miR-135 had to be perfectly complementary to the target gene 3'-UTR, and the binding site had to be conserved across mammalian species (conservation score ≥ 0.6). False-positive control strategies: (1) Only high-scoring targets with context++ score ≤ -0.20 were included; (2) Perfect seed sequence matching was required; (3) Binding sites not conserved across multiple species were filtered out. *Prediction results*: TargetScan predicted a high-confidence binding site for miR-135 at nucleotides 456-462 (sequence: 5'-ACTGTAA-3') of the CD44v6 3'-UTR (GenBank accession: NM_001001391.2), with a context++ score of -0.23 (percentile: 93). The binding site was highly conserved across human, mouse and rat (conservation score: 0.82).

Dual-luciferase reporter assay

The potential binding site of miR-135 in the CD44v6 3'-UTR was predicted using TargetScan (version 7.2). The wild-type (WT) CD44v6 3'-UTR fragment containing the predicted binding site was amplified by PCR and cloned into the pmirGLO dual-luciferase reporter vector (Promega, USA) downstream of the firefly luciferase gene to construct the pMIR-CD44v6-WT recombinant plasmid. For mutant (MUT) construction, the binding site of the miR-135 seed sequence (positions 2-8) was mutated from 5'-ACTGTAA-3' to 5'-AAGCTTT-3' using a site-directed mutagenesis kit (QuikChange II, Agilent, USA) to disrupt miRNA-mRNA complementarity, generating the pMIR-CD44v6-MUT plasmid. All constructs were verified by Sanger sequencing. For cell transfection, HEK293T cells were seeded into 96-well plates at a density of 1×10^4 cells per well. After 24 hours, co-transfection was performed using Lipofectamine 2000 (Invitrogen, USA). Each well contained 100 ng of reporter plasmid (WT or MUT), 50 ng of miR-135 mimic or NC mimic and 10 ng of pRL-TK internal control plasmid (expressing Renilla luciferase for normalization). Six replicate wells were set per group. For luciferase activity detection, 48 hours after transfection, firefly and Renilla luciferase activities were measured using the Dual-Luciferase Reporter Assay System (Promega, USA) with a SpectraMax iD3 microplate reader (Molecular Devices, USA). For data normalization, the firefly luciferase activity of each well was divided by its Renilla luciferase activity to obtain the relative luciferase activity (RLA). RLA values of each experimental group were then normalized to the NC mimic group (set to 1.0). Each experiment was independently repeated 3 times (n=3), with 6 technical replicates per experiment. Data are presented as mean ± standard deviation (SD). Comparisons between two groups were performed using two-tailed Student's *t*-test. Statistical significance was set at $*p* < 0.05$.

CCK-8 assay

Twenty-four hours after transfection, cells were collected and seeded into 96-well plates at a density of 5×10^3 cells per well in 100 μL of medium. At 24, 48 and 72 hours after seeding, 10 μL of CCK-8 reagent (Dojindo, Japan, catalog No. CK04) was added to each well, followed by incubation at 37°C in 5% CO_2 for 2 hours in the dark. Absorbance at 450 nm was measured using a multi-mode microplate reader (Bio-Rad, USA). Cell viability was normalized to the untreated control group (0 μmol/L cisplatin). Five replicate wells were set per group and the experiment was independently repeated three times.

Cisplatin IC50 determination

The CCK-8 assay was used to determine the half-maximal inhibitory concentration (IC50) of cisplatin for each cell group. Cells (HeLa parental cells, HeLa/DDP cells transfected with NC mimic and HeLa/DDP cells transfected with miR-135 mimic) in logarithmic growth phase were seeded into 96-well plates at a density of 5 × 10^3 cells per well in 100 μL of medium. After 24 hours of culture, the medium was replaced with fresh medium containing cisplatin at gradient concentrations (0, 1, 2.5, 5, 10, 25, 50, 100 μmol/L), with three replicate wells per concentration. After 48 hours of culture, 10 μL of CCK-8 reagent was added to each well, followed by incubation at 37°C in 5% CO_2 for 2 hours in the dark. Absorbance at 450 nm was measured using a microplate reader. Cell viability (%) = (ODexperimental - ODblank) / (ODcontrol - ODblank) × 100%. IC50 values and 95% confidence intervals (CI) were calculated by nonlinear regression (four-parameter variable slope model) fitting of dose-response curves using GraphPad Prism 9.0 software. Each experiment was independently repeated three times.

Western blot analysis

Protein extraction: Cells from each group were collected and proteins were extracted using RIPA lysis buffer (containing 1% PMSF and protease inhibitor cocktail) on ice for 30 minutes, followed by centrifugation at 12,000 rpm for 15 minutes. The supernatant was collected. *Protein quantification*: Protein concentration was determined using the BCA protein assay kit (Thermo Fisher, USA). *Electrophoresis and transfer:* 30 μg of protein per sample were separated by 10% SDS-PAGE and then transferred to PVDF membranes (Millipore, USA) at a constant current of 300 mA for 90 minutes. Blocking and incubation: Membranes were blocked with 5% non-fat milk at room temperature for 1 hour. Primary antibodies were incubated overnight at 4°C including mouse anti-CD44v6 monoclonal antibody (clone VFF-7, 1:200) and rabbit anti-β-actin (1:1000). The next day, membranes were washed three times with TBST (10 minutes each), followed by incubation with secondary antibodies at room temperature for 1 hour. *Detection:* Blots were visualized using enhanced ECL chemiluminescence reagent (GE Healthcare, UK) and images were captured using a C-DiGit scanner (LI-COR, USA). *Densitometric quantification:* Band intensities were analyzed using ImageJ software (NIH, USA). Relative protein expression = (target protein gray value / internal control gray value) experimental group / (target protein gray value / internal control gray value) control group. The primary antibody for CD44v6 was a mouse monoclonal antibody (clone VFF-7, catalog No. ab119863, Beijing Sipaerke), which specifically recognizes the v6 variant exon of human CD44 and does not cross-react with the standard CD44s isoform. GAPDH antibody was used as a loading control.

Flow cytometry for detecting apoptosis

Cell processing: Forty-eight hours after transfection, cells from each group (NC mimic group, miR-135 mimic group) were collected. Cells were gently detached using 0.25% trypsin without EDTA to avoid mechanical damage and collected in 15 mL centrifuge tubes. *Cell washing:* Cells were centrifuged at 1000 rpm for 5 minutes, the supernatant was discarded and cells were resuspended in 2 mL of pre-chilled PBS. Centrifugation was repeated twice. *Staining:* The Annexin V-FITC/PI Apoptosis Detection Kit (BD Biosciences, USA, catalog No. 556547) was used. Cells were resuspended in 1× Binding Buffer at a concentration of 1 × 10^6 cells/mL. One hundred microliters of cell suspension (containing 1 × 10^5 cells) were transferred to flow cytometry tubes, followed by sequential addition of 5 μL of Annexin V-FITC and 5 μL of PI staining solution, with gentle mixing. *Incubation:* The mixture was incubated at room temperature for 15 minutes in the dark. After incubation, 400 μL of 1× binding buffer was added to each tube, followed by gentle mixing. *Flow cytometry analysis:* Samples were analyzed within 1 hour using a FACS Calibur flow cytometer (BD Biosciences, USA). The excitation wavelength was 488 nm, with FITC detected in the FL1 channel (530 nm) and PI detected in the FL2 channel (585 nm). A total of 10,000 events were collected per sample. *Data analysis:* Data were analyzed using FlowJo software (version 10.8). Cell debris and doublets were excluded by FSC/SSC gating. Based on Annexin V-FITC/PI double staining, cells were divided into four populations including lower left quadrant (Q3): Annexin V^-/PI^- (live cells), lower right quadrant (Q4): Annexin V^+/PI^- (early apoptotic cells), upper right quadrant (Q2): Annexin V^+/PI^+ (late apoptotic cells) and upper left quadrant (Q1): Annexin V^-/PI^+ (necrotic cells). Apoptosis rate (%) = early apoptosis rate (Q4) + late apoptosis rate (Q2). Each group had three replicate wells and the experiment was independently repeated three times.

Clone formation assay

Forty-eight hours after transfection, cells from each group were collected and seeded into 6-well plates at a density of 500 cells per well in 2 mL of complete medium. Cells were cultured at 37°C in 5% CO_2 for 10-14 days, with medium changed every 3 days. When visible colonies appeared (>50 cells), the medium was discarded, cells were washed twice with PBS, fixed with 4% paraformaldehyde for 15 minutes and stained with 0.1% crystal violet for 20 minutes. Excess dye was gently rinsed off with deionized water and plates were air-dried. Colonies were photographed under an inverted microscope and counted using ImageJ software (colonies with ≥50 cells were counted). Colony formation rate (%) = (number of colonies/number of cells seeded) × 100%. Each group had three replicate wells and the experiment was independently repeated three times.

Statistical analysis

All experiments were independently repeated three times (n = 3), with three technical replicates per independent experiment (unless otherwise specified). Biological replicates refer to independently performed cell experiments, while technical replicates refer to parallel samples within the same experiment. Data are presented as mean ± standard deviation (SD). Error bars in all figures represent SD, not standard error of the mean (SEM). *Normality testing:* Before parametric tests, the Shapiro-Wilk test was used to assess whether the data were normally distributed. If *p* > 0.05, the data were considered normally distributed. All data in this study met the assumption of normality ($p > 0.05$). *Homogeneity of variance testing:* For two-group comparisons, Levene's test was used to assess homogeneity of variance. If variances were unequal, Welch's corrected t-test was used.

Statistical tests: Two-group comparisons: When data were normally distributed with homogeneous variances, a two-tailed Student's t-test was used; when variances were unequal, Welch's corrected t-test was used. Multi-group comparisons: A one-way ANOVA followed by Tukey's post hoc test was used to compare groups. *IC50 calculation:* IC50 values were calculated by nonlinear regression (four-parameter variable slope model) fitting of dose-response curves and 95% confidence intervals (CI) were reported. *Effect size reporting:* Two-group comparisons: Cohen's d was reported, with thresholds: d ≥ 0.2 (small effect), ≥ 0.5 (medium effect), ≥ 0.8 (large effect). *Multi-group comparisons:* η^2 (eta-squared) was reported, with thresholds of $\eta^2 \geqslant 0.01$ (small effect), ⩾ 0.06 (medium effect) and ≥ 0.14 (large effect). *p-value reporting:* Exact *p-values* were reported to three decimal places (e.g., p = 0.023). For extremely small p-values, p < 0.001 was uniformly reported. The significance level was set at $\alpha = 0.05$, with $p < 0.05$ considered statistically significant. *Normalization methods:* qRT-PCR: Relative expression was calculated using the $2^{-\Delta\Delta Ct}$ method, with the control group set to 1.0. ΔCt = Ct(target gene) - Ct(internal control), ΔΔCt = ΔCt(experimental group) - ΔCt(control group). Western blot: The gray value of the target protein was normalized to that of GAPDH and the ratio was then normalized to the control group (set to 1.0).

Dual-luciferase reporter assay: Firefly luciferase activity of each well was divided by Renilla luciferase activity to obtain relative luciferase activity (RLA). RLA values of experimental groups were then normalized to the NC mimic group (set to 1.0). CCK-8: OD values at each concentration were normalized to the untreated control (0 μmol/L cisplatin) to calculate cell survival percentage. *Quantitative index calculations:* Resistance Index (RI) = IC50(resistant cells) / IC50(parental cells).Resistance reversal fold = IC50(NC mimic group) / IC50(miR-135 mimic group). Luciferase inhibition percentage = (1 - RLAexperimental / RLAControl) × 100%. Apoptosis rate = early apoptosis rate (Annexin V^+/PI^-) + late apoptosis rate (Annexin V^+/PI^+). Colony formation rate = (number of colonies/number of cells seeded) × 100%. *Software:* Statistical analyses and graph generation were performed using GraphPad Prism 9.0 (GraphPad Software, San Diego, CA, USA).

RESULTS

miR-135 targets CD44v6

TargetScan predicted complementarity between the seed sequence of miR-135 and the CD44v6 3'-UTR (Fig. 1A). To validate this interaction, dual-luciferase reporter plasmids containing the wild-type (WT) or seed sequence mutant (MUT) CD44v6 3'-UTR were constructed (Fig. 1B). The dual-luciferase reporter assay (Fig. 1C) showed that after transfection with the wild-type (WT) reporter plasmid, the relative luciferase activity (RLA) of the miR-135 mimic group was 0.42 ± 0.06 (95% CI: 0.36 – 0.48), while that of the NC mimic group was 1.00 ± 0.05 (95% CI: 0.95 – 1.05). Compared with the NC mimic group, the miR-135 mimic group showed a 58% reduction in RLA (fold change = 0.42, 95% CI for difference: 0.52 – 0.64, $p < 0.001$, Cohen's d = 4.2, large effect size).

After transfection with the mutant (MUT) reporter plasmid, no significant difference was observed between the two groups (0.96 ± 0.07 vs. 1.00 ± 0.05, p = 0.452, Cohen's d = 0.32, small effect size), confirming the specificity of the binding site. qRT-PCR results (Fig. 1D) showed no significant change in CD44v6 mRNA levels after miR-135 overexpression (miR-135 mimic group vs. NC mimic group: 1.02 ± 0.06 vs. 1.00 ± 0.05, p = 0.673, Cohen's d = 0.15, small effect size). Western blot results (Fig. 1E) showed that after miR-135 mimic transfection, CD44v6 protein expression was reduced by 62% compared with the NC mimic group (NC mimic: 1.00 ± 0.08, 95% CI: 0.92 – 1.08; miR-135 mimic: 0.38 ± 0.05, 95% CI: 0.33 – 0.43; fold change = 0.38, 95% CI for difference: 0.52 – 0.72, $p < 0.001$, Cohen's d= 3.2, large effect size).

Validation of CD44v6-specific detection tools

Western blot results (Fig. 2A) showed that the VFF-7 antibody detected a single band at approximately 85 kDa, consistent with the predicted molecular weight of CD44v6, while no band was observed after pre-incubation of the antibody with the blocking peptide. qRT-PCR results (Fig. 2B) showed that the CD44v6-specific primers amplified a single band of the expected size (142 bp), with no amplification in the no-template control (NTC). Sanger sequencing further confirmed the specificity of the amplified product (Fig. 2C).

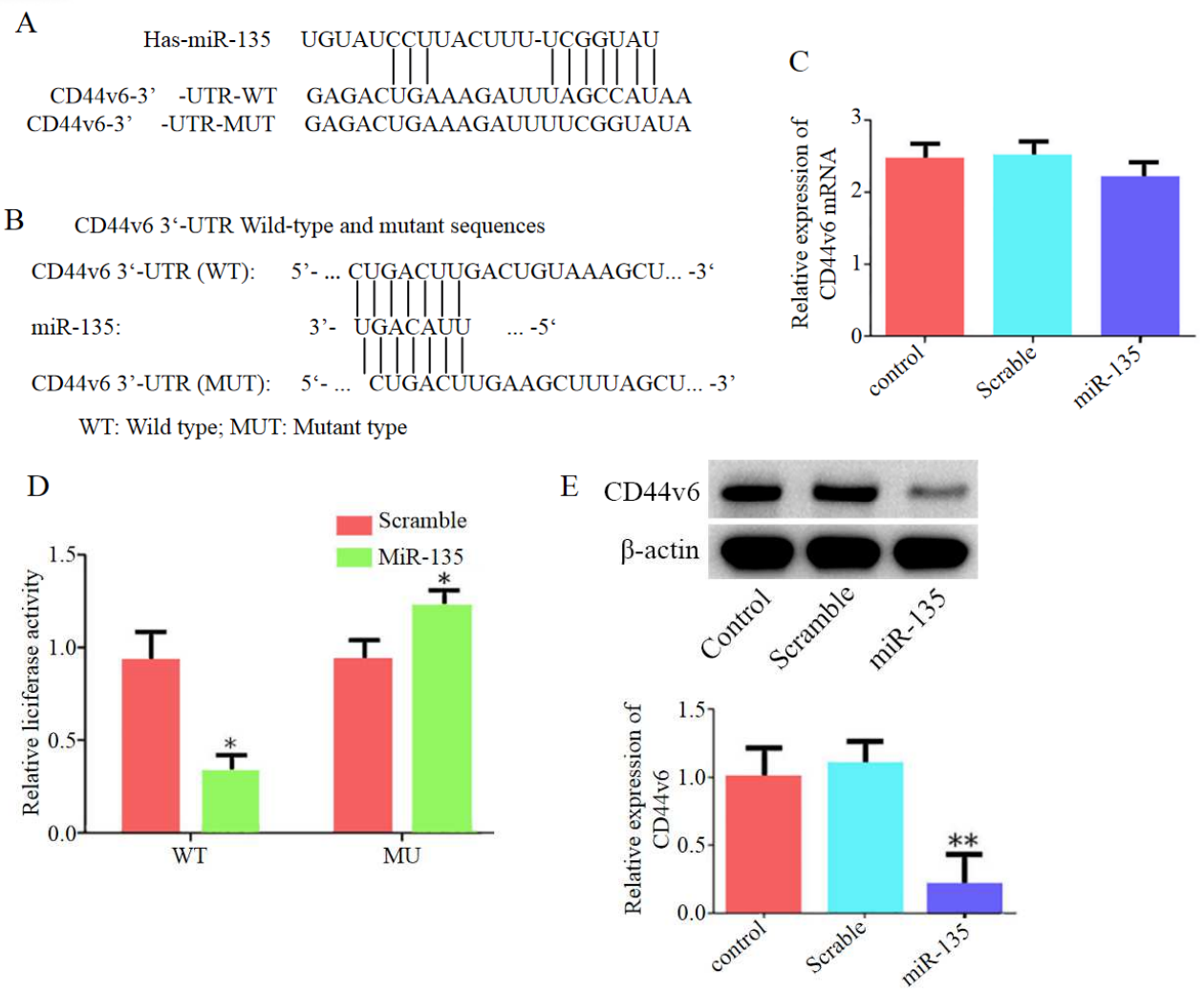

Fig. 1: miR-135 targets CD44v6.

(A) Schematic diagram of the predicted binding site between miR-135 and the CD44v6 3'-UTR; (B) Schematic representation of the dual-luciferase reporter constructs. The pRL-TK plasmid, constitutively expressing Renilla luciferase, was used as an internal control for normalization; (C) Dual-luciferase reporter assay. Firefly luciferase activity was normalized to Renilla luciferase activity and values were then normalized to the NC mimic group (set to 1.0). Data are presented as mean ± SD (n=3 independent experiments, each with 6 technical replicates). *p < 0.05, **p < 0.01, ***p < 0.001 vs. NC mimic group (two-tailed Student's t--test); (D) qRT-PCR analysis of CD44v6 mRNA expression in HeLa cells transfected with NC mimic or miR-135 mimic. GAPDH was used as an internal control. Data are presented as mean ± SD (n=3 independent experiments); (E) Western blot analysis of CD44v6 protein expression in HeLa cells transfected with NC mimic or miR-135 mimic. GAPDH was used as a loading control. Representative blots from three independent experiments are shown. *p < 0.05, **p < 0.01, ***p < 0.001 vs. NC mimic group (two-tailed

Proliferation of drug-resistant cells is enhanced

The MTT assay showed that HeLa/DDP cells exhibited higher proliferative capacity than parental HeLa cells at all time points (Fig. 3A). Under treatment with increasing concentrations of cisplatin, HeLa/DDP cells showed significantly higher viability than parental HeLa cells (Fig. 3B). The colony formation assay (Fig. 3C) further confirmed that the colony-forming ability of HeLa/DDP cells was increased by 3.2-fold compared with HeLa cells (HeLa/DDP: 156 ± 12 colonies, HeLa: 49 ± 6 colonies, $p < 0.01$, Cohen's $d = 2.9$, large effect size).

miR-135 expression is decreased while CD44v6 is increased in drug-resistant cells

qRT-PCR results (Fig. 4A) showed that compared with normal Ect1/E6E7 cells (1.00 ± 0.06, 95% CI: 0.94 – 1.06), miR-135 expression in HeLa/DDP cells was reduced by 68%, with a relative expression level of 0.32 ± 0.05 (95% CI: 0.27 – 0.37) (fold change = 0.32, 95% CI for difference: 0.55 – 0.81, $p < 0.01$, Cohen's $d = 3.1$, large effect size). Conversely, CD44v6 mRNA expression was significantly increased (Fig. 4B).

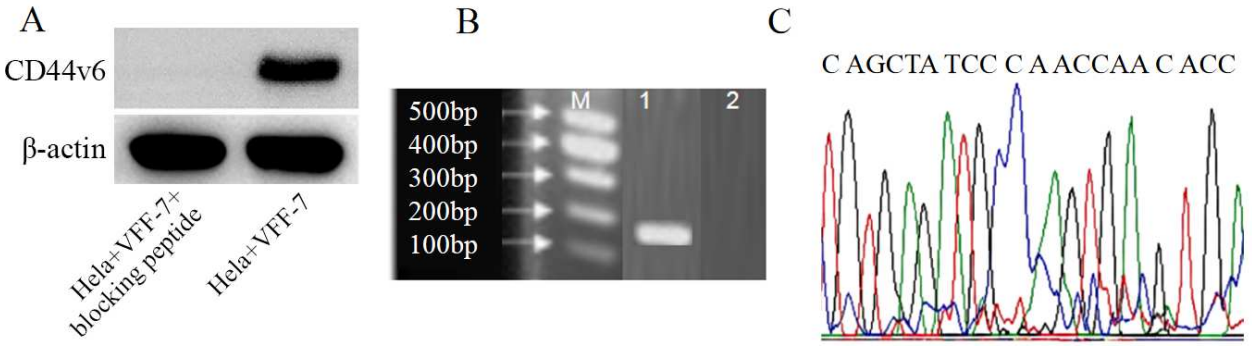

Fig. 2: Validation of CD44v6-specific detection tools.
(A) Western blot analysis of CD44v6 expression in HeLa cell lysates using VFF-7 antibody. Lane 1: Normal detection, showing a single band at approximately 85 kDa; Lane 2: Antibody pre-incubated with blocking peptide, showing no band (negative control). β-actin served as a loading control; (B) Agarose gel electrophoresis of qRT-PCR products using CD44v6-specific primers. Lane M: DNA marker (100, 200, 300, 400, 500 bp); Lane 1: HeLa cell cDNA template, showing a single band at approximately 140 bp, consistent with the expected product size (142 bp); Lane 2: No-template control (NTC), showing no amplification; (C) Sanger sequencing chromatogram of the qRT-PCR product. The sequencing result (5'-CAGCTATCCCAACCAACACC-3') showed 100% identity with the CD44v6 reference sequence (GenBank NM_001001391.2), confirming specific amplification of the CD44v6 transcript.

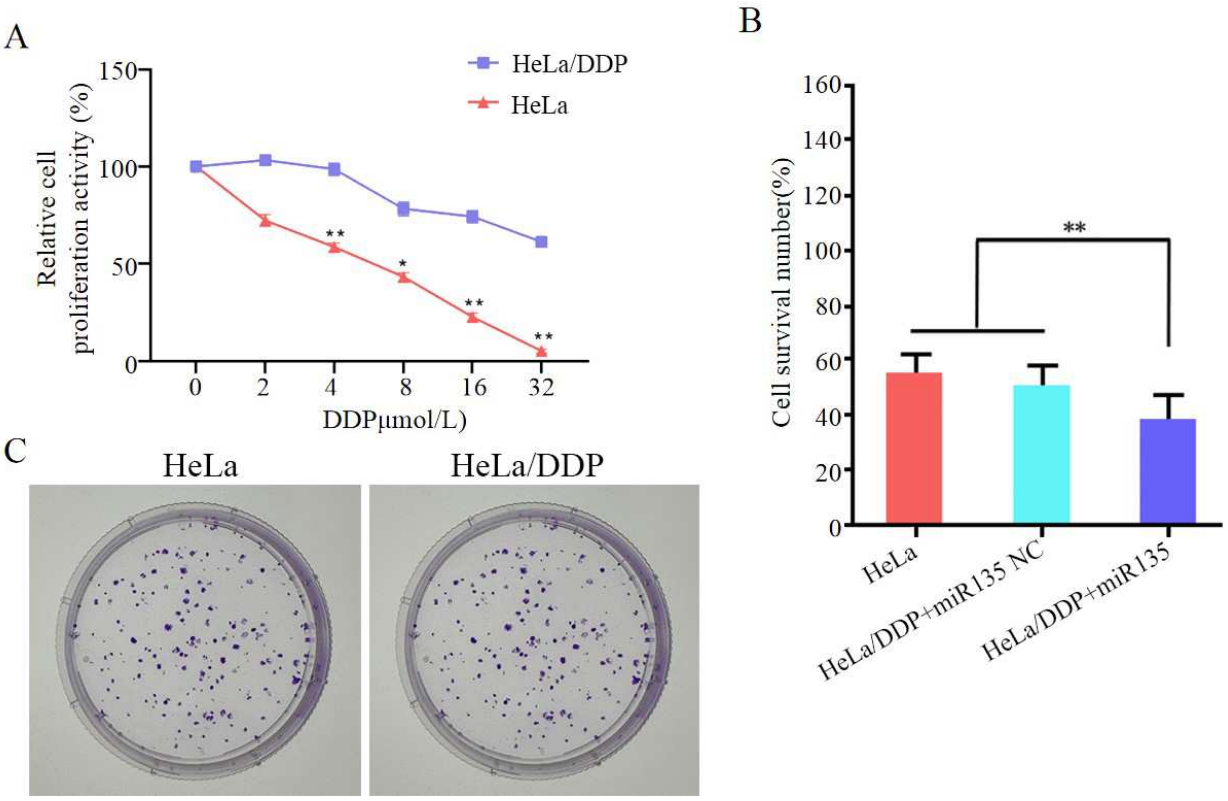

Fig. 3: The proliferation of drug-resistant cell is enhanced.
(A) MTT assay of proliferative capacity of HeLa and HeLa/DDP cells; (B) Cell viability after treatment with increasing concentrations of cisplatin for 48 hours; (C) Colony formation assay. Data are presented as mean ± SD (n=3 independent experiments). *p < 0.05, **p < 0.01, ***p < 0.001 vs. HeLa parental cells (two-tailed Student's t--test).

The relative CD44v6 mRNA expression level in HeLa/DDP cells was 3.80 ± 0.40 (95% CI: 3.40 – 4.20), while that in the Ect1/E6E7 group was 1.00 ± 0.08 (95% CI: 0.92 – 1.08). Compared with the Ect1/E6E7 group, CD44v6 mRNA in HeLa/DDP cells was increased by 2.8-fold (fold change = 3.80, 95% CI for difference: 2.40 – 5.20, p < 0.01, Cohen's d = 2.8, large effect size). Western blot analysis further confirmed (Fig. 4C) that the relative

CD44v6 protein expression level in HeLa/DDP cells was 3.50 ± 0.08 (95% CI: 3.42 – 3.58), while that in the Ect1/E6E7 group was 1.00 ± 0.02 (95% CI: 0.98 – 1.02). Compared with the Ect1/E6E7 group, CD44v6 protein in HeLa/DDP cells was increased by 2.5-fold (fold change = 3.50, 95% CI for difference: 2.42 – 4.58, $p < 0.01$, Cohen's d = 3.5, large effect size).

miR-135 overexpression reverses cisplatin resistance in HeLa/DDP cells

As shown in table 1, the cisplatin IC50 value of HeLa/DDP cells was 22.36 μmol/L (95% CI: 20.15 – 24.57 μmol/L), while that of HeLa parental cells was 4.57 μmol/L (95% CI: 3.98 – 5.16 μmol/L). The Resistance Index = 22.36 / 4.57 = 4.89, indicating that the cisplatin resistance of HeLa/DDP cells was approximately 4.9-fold that of parental cells ($p < 0.001$, Cohen's d = 3.8, large effect size). As shown in fig. 5A, the dose-response curve of the miR-135 mimic group was significantly left-shifted compared with the NC mimic group, suggesting enhanced sensitivity to cisplatin. As shown in fig. 5B, after transfection of HeLa/DDP cells with miR-135 mimic, the cisplatin IC50 value significantly decreased to 8.47 μmol/L (95% CI: 6.92 – 9.93 μmol/L), while that of the NC mimic group was 22.36 μmol/L (95% CI: 20.15 – 24.57 μmol/L). Compared with the NC mimic group, miR-135 mimic transfection reduced the IC50 by 62%, with a resistance reversal fold of 2.64 (95% CI for difference: 11.23 – 16.55 μmol/L, $p < 0.001$, Cohen's d = 4.2, large effect size).

miR-135 overexpression inhibits proliferation and induces apoptosis in HeLa/DDP cells

As shown in fig. 6A, after transfection, miR-135 expression increased by 4.2-fold (miR-135 mimic group vs. NC mimic group: 4.20 ± 0.35 vs. 1.00 ± 0.08, $p < 0.001$, Cohen's d = 3.5, large effect size). Correspondingly, CD44v6 mRNA expression decreased by 62% (Fig. 6B), with a relative expression level of 0.38 ± 0.04 (95% CI: 0.34 – 0.42), while the NC mimic group was 1.00 ± 0.06 (95% CI: 0.94 – 1.06) (fold change = 0.38, 95% CI for difference: 0.52 – 0.72, $p < 0.001$, Cohen's *d* = 3.2, large effect size). Western blot confirmed that CD44v6 protein expression decreased by 61% (Fig. 6C). Densitometric analysis showed that the relative CD44v6 protein expression level in the miR-135 mimic group was 0.39 ± 0.03 (95% CI: 0.36 – 0.42), while that in the NC mimic group was 1.00 ± 0.05 (95% CI: 0.95 – 1.05) (fold change = 0.39, 95% CI for difference: 0.51 – 0.69, $p < 0.001$, Cohen's d = 3.8, large effect size). Functional assays showed that miR-135 mimic transfection significantly inhibited cell proliferation (Fig. 6D). CCK-8 assay showed that 48 hours after transfection, cell viability in the miR-135 mimic group was 43.7% ± 5.2% (95% CI: 38.5% – 48.9%), while that in the NC mimic group was 100.0% ± 8.0% (95% CI: 92.0% – 108.0%). Compared with the NC mimic group, miR-135 mimic transfection reduced cell viability by 56.3% (fold change = 0.44, 95% CI for difference: 0.32 – 0.56, $p < 0.001$, Cohen's d = 2.5, large effect size). Flow cytometry (Fig. 6E) showed that transfection with the miR-135 mimic significantly induced apoptosis in HeLa/DDP cells. The apoptosis rate in the miR-135 mimic group was 35.8% ± 3.2% (95% CI: 32.6% – 39.0%), while that in the NC mimic group was 12.4% ± 1.8% (95% CI: 10.6% – 14.2%). Compared with the NC mimic group, miR-135 mimic transfection increased the apoptosis rate by an absolute 23.4% (95% CI for difference: 18.2% – 28.6%), representing a relative increase of 2.9-fold (fold change = 2.89, $p < 0.001$, Cohen's d = 4.5, large effect size).

DISCUSSION

Cisplatin, a non-specific anticancer drug, is widely used to treat human solid tumors (Gong *et al*., 2025). Cisplatin induces cell apoptosis by activating ATR, p53, MAPK and other signaling pathways (Zhang H *et al*., 2025). However, the effect of cisplatin on apoptosis diminishes over time, leading to drug resistance, the main challenge of chemotherapy. In CC, multiple miRNAs have been shown to be aberrantly expressed and involved in key processes such as proliferation, apoptosis, invasion and drug resistance (Feitosa *et al*., 2024). A cohort study demonstrated that differential miRNA expression was significantly associated with poor treatment response to chemoradiotherapy and shorter overall survival (Julianti *et al*., 2026), suggesting that miRNAs may serve as potential therapeutic targets in CC. However, the specific role of miR-135 in cisplatin-resistant CC remains unclear. The current study confirmed that miR-135 was overexpressed in drug-resistant CC cells compared with non-drug-resistant CC cells, suggesting that miR-135 may be involved in CC drug resistance. Previously, miR-135 has been implicated as downregulated in various cancers, where it exerts tumor-suppressive activity through p53-related mechanisms and by inactivating signal transduction pathways through downregulation of the target gene HOXA10 (Kadkhoda *et al*., 2022; Babaei-Jadidi *et al*., 2022).

CD44v6 is widely expressed across various cell types (Ghatak *et al*., 2022a). High CD44v6 expression has been associated with poor prognosis in breast and colon cancers (Ejima *et al*., 2023). CD44v6 may function as an oncogenic factor that induces drug resistance in liver, prostate, oral squamous cell, and other cancer cells. Although the expression and functional behavior of CD44v6 have been elucidated in colon cancer, its biological effects on CC metastasis and drug resistance remain unclear (Hirayama *et al*., 2025; Chen *et al*., 2025).

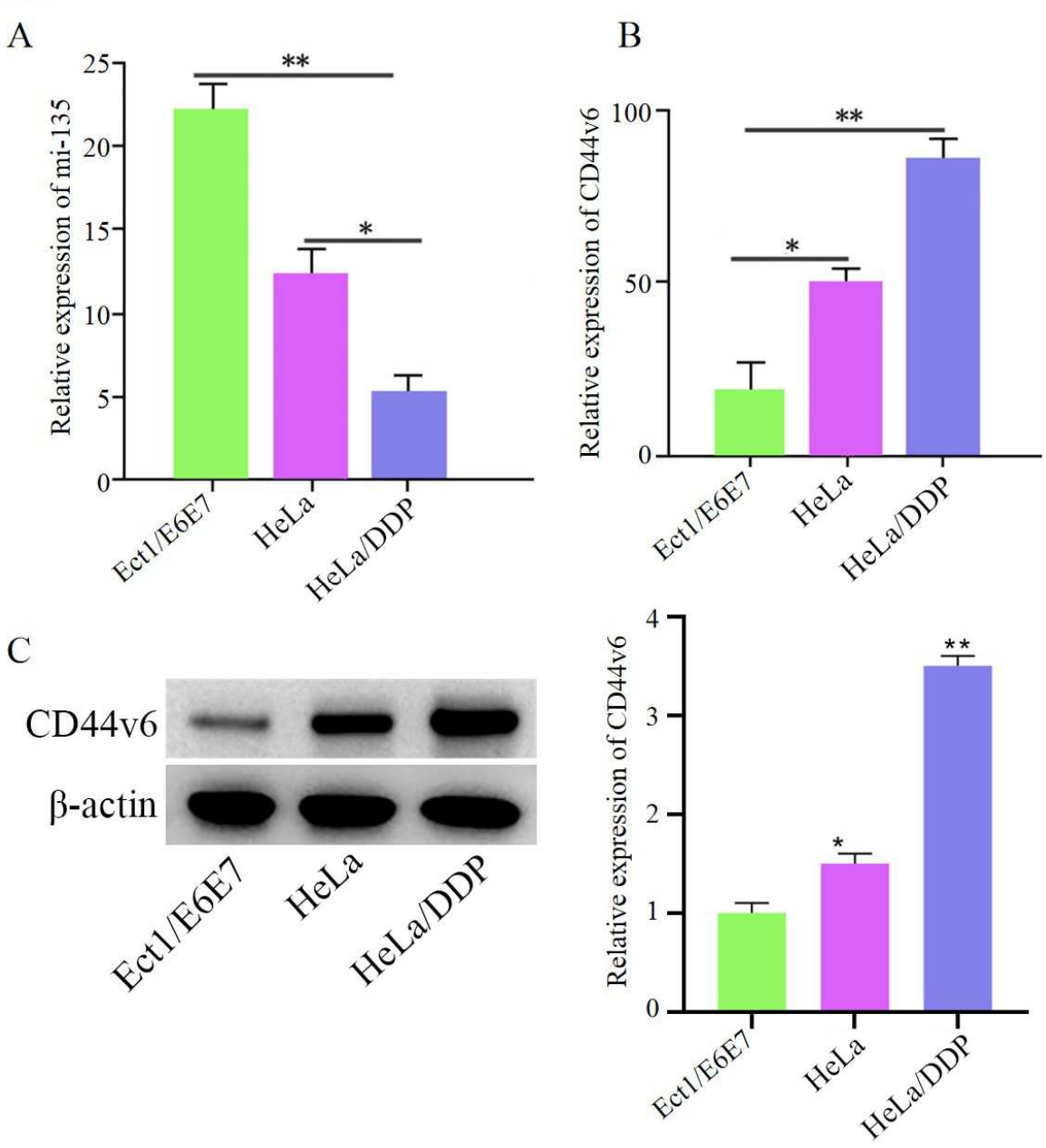

Fig. 4: miR-135 expression is decreased while CD44v6 is increased in drug-resistant cells.
(A) qRT-PCR analysis of miR-135 expression. U6 was used as an internal control. Data are presented as mean ± SD (n=3 independent experiments). *p < 0.05, **p < 0.01, ***p < 0.001 vs. Ect1/E6E7 cells (two-tailed Student's t--test); (B) qRT-PCR analysis of CD44v6 mRNA expression. GAPDH was used as an internal control. Data are presented as mean ± SD (n=3 independent experiments). *p < 0.05, **p < 0.01, ***p < 0.001 vs. Ect1/E6E7 cells (two-tailed Student's t--test); (C) Western blot analysis of CD44v6 protein expression. Data are presented as mean ± SD (n=3 independent experiments). *p < 0.05, **p < 0.01, ***p < 0.001vs. Ect1/E6E7 cells (two-tailed Student's t--test).

Table 1: Characteristics of the cisplatin-resistant cell model.

Parameter	HeLa parental	HeLa/DDP	RI / Fold-change
IC50 (μmol/L)	4.57	22.36	RI = 4.89
95% CI (μmol/L)	3.98 – 5.16	20.15 – 24.57	≈ 4.9-fold
Stability (passages)	–	10–20	Validated every 5 passages
Maintenance	–	1.0 μmol/L cisplatin	Withdrawn 7 days pre-experiment

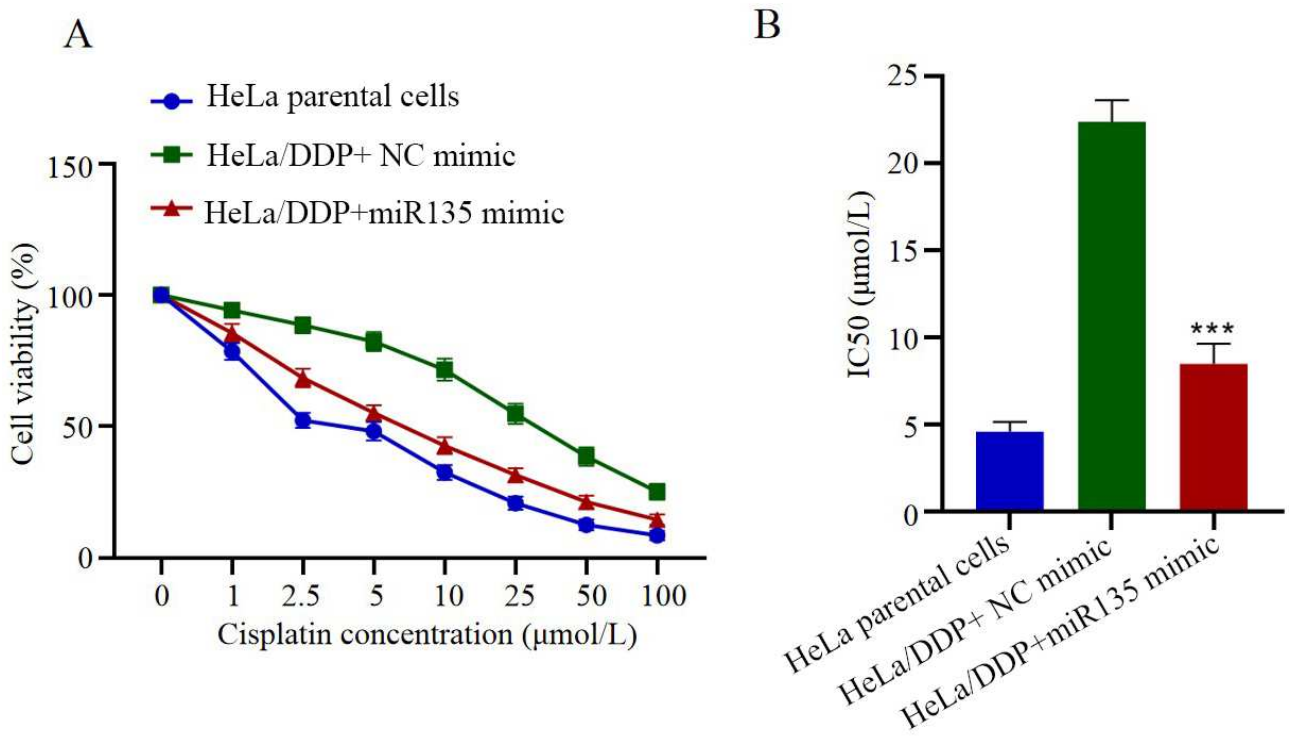

Fig. 5: miR-135 overexpression reduces cisplatin IC50 in HeLa/DDP cells.
(A) Dose-response curves of HeLa parental cells, HeLa/DDP cells transfected with NC mimic or miR-135 mimic after 48 h of cisplatin treatment. Data are presented as mean ± SD (n=3 independent experiments); (B) Cisplatin IC50 values of each group. *p < 0.05，**p < 0.01，***p < 0.001 vs. NC mimic group (two-tailed Student's t--test).

In this study, the binding relationship between CD44v6 and miR-135 was confirmed, as transfection with a miR-135 mimic reduced relative luciferase activity in cells transfected with pMIR-CD44v6-WT. It should be noted that the dual-luciferase reporter assay works by cloning the target gene's 3'-UTR downstream of the firefly luciferase reporter gene and co-transfecting cells with the miRNA mimic and the Renilla luciferase internal control plasmid; if the miRNA binds complementarily to the target sequence, it inhibits firefly luciferase translation, leading to decreased activity, which is normalized to Renilla luciferase to assess binding strength quantitatively (Queffeulou *et al*., 2025). This study used this technique to directly validate the physical interaction between miR-135 and the CD44v6 3'-UTR and mutation experiments were performed to exclude non-specific binding, providing a reliable basis for subsequent functional studies. The IC50 value of drug-resistant cells was significantly higher than that of parental CC cells, indicating successful establishment of DDP-resistant CC cells. qRT-PCR and Western blot analyses indicated downregulated miR-135 expression and upregulated CD44v6 expression in CC cells compared to normal cervical epithelial cells. Moreover, miR-135 expression in drug-resistant CC cells was even lower than that in non-drug-resistant CC cells, while CD44v6 mRNA expression was enhanced. These data suggest that miR-135 might alleviate CC progression by inhibiting CD44v6 expression and drug resistance in CC cells. Previous studies have also highlighted the relationship between miR-135 and CC, with downregulated miR-135 expression associated with CC tumor growth and oxaliplatin resistance (Shiri Aghbash *et al*., 2023). Consistently, the *in vitro assays in* the present study showed that miR-135 was poorly expressed in CC cells and further decreased in drug-resistant CC cells (Wise *et al*., 2024).

Meanwhile, CD44v has also been highlighted in CC. For example, CD44v levels in the serum and plasma of CC patients were elevated (Suwiwat *et al*., 2022). In addition, aberrant CD44v expression in CC tissues was positively correlated with tumor invasion (Lodewijk *et al*., 2023).

In line with previous studies, this study also showed that the abnormal increase in CD44v was associated with CC. Furthermore, studies in breast cancer demonstrated that CD44v expression could effectively predict proliferative activity, with the CD44v3 subtype particularly positively correlated with drug resistance in breast cancer (Kundu *et al*., 2024). This research also indicated a significant correlation between CD44v6 and drug resistance.

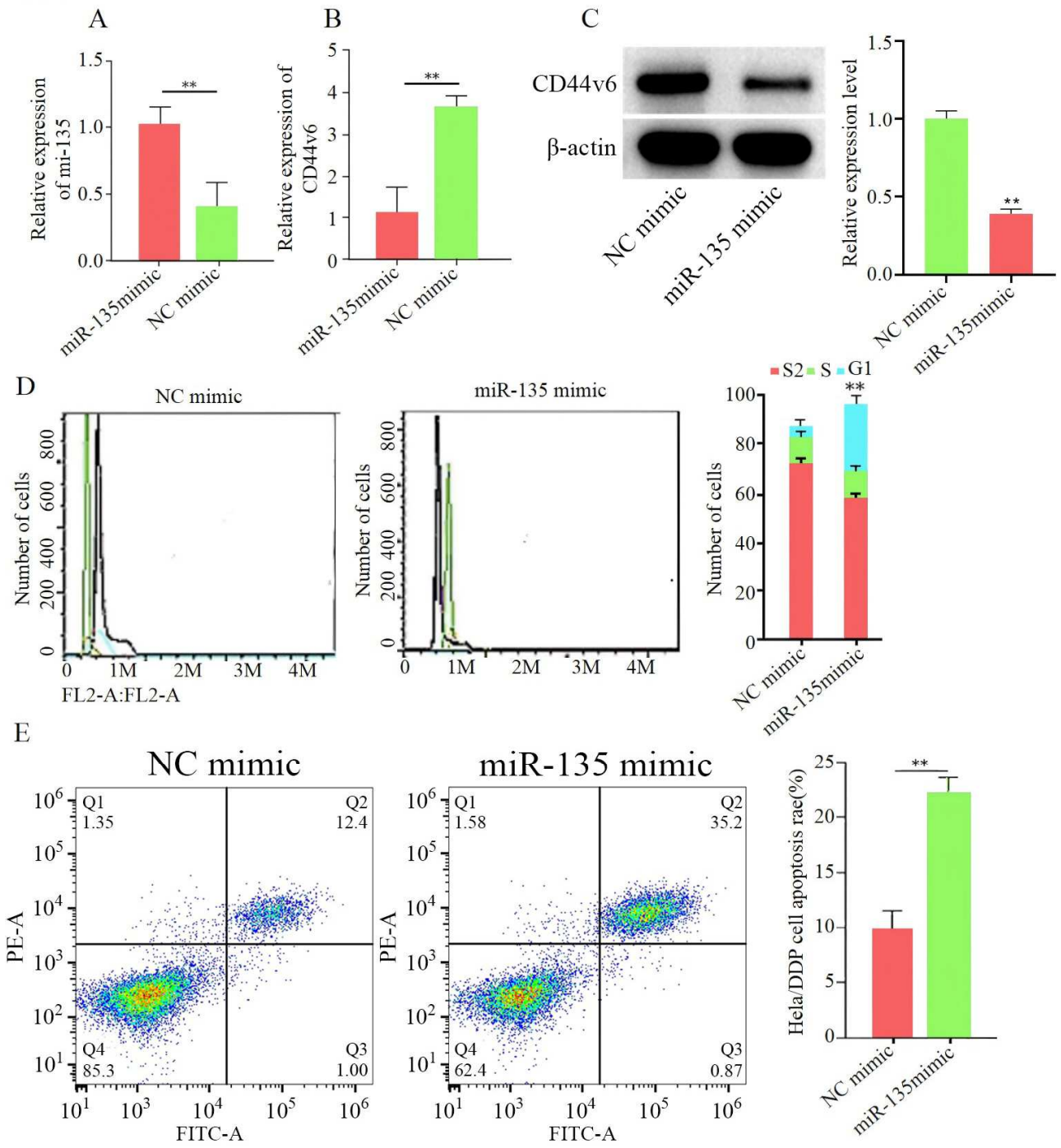

Fig. 6: miR-135 inhibits the progression of CC cells.
(A) qRT-PCR analysis of miR-135 expression. U6 was used as an internal control. Data are presented as mean ± SD (n=3 independent experiments). *p < 0.05, **p < 0.01, ***p < 0.001vs. NC mimic group (two-tailed Student's t--test); (B) qRT-PCR analysis of CD44v6 mRNA expression. GAPDH was used as an internal control. Data are presented as mean ± SD (n=3 independent experiments). *p < 0.05, **p < 0.01, ***p < 0.001 vs. NC mimic group (two-tailed Student's t--test); (C) Western blot analysis of CD44v6 protein expression. Data are presented as mean ± SD (n=3 independent experiments). *p < 0.05, **p < 0.01, ***p < 0.001vs. NC mimic group (two-tailed Student's t--test); (D) CCK-8 assay for cell proliferation. Data are presented as mean ± SD (n=3 independent experiments). *p < 0.05, **p < 0.01, ***p < 0.001 vs. NC mimic group (two-tailed Student's t--test); (E) Flow cytometry for cell apoptosis. Data are presented as mean ± SD (n=3 independent experiments). *p < 0.05, **p < 0.01, ***p < 0.001 vs. NC mimic group (two-tailed Student's t--test).

This study assessed whether miR-135 could affect DDP resistance by regulating CD44v6. As a consequence, transfection with a miR-135 mimic reduced CD44v6 expression and increased apoptosis in drug-resistant cells, thereby diminishing DDP resistance. Relevant studies have shown that in breast cancer, miR-135 overexpression increases p-GSK3β expression and decreases Wnt and β-catenin expression, thereby inactivating the Wnt/β-catenin pathway to inhibit tumor progression (Peng *et al*., 2021). This is highly consistent with the functional phenotype observed in this study, in which miR-135 overexpression inhibited CC cell proliferation and induced apoptosis, supporting its cross-tumor role as a tumor-suppressive miRNA. In contrast, in esophageal cancer, cisplatin treatment reduces miR-135b-5p expression, and overexpression of miR-135b-5p attenuates the cytotoxic effects of cisplatin (Di et al., 2021), which is the opposite of the findings of this study and others. This suggests that miR-135's function may be tumor type-specific. Furthermore, relevant studies have shown that CD44 genetic polymorphisms are significantly associated with poorer 5-year survival (HR = 3.30, 95% CI: 1.28-8.49) and CC risk (HR = 10.29, 95% CI: 1.18-89.40) in CC patients (Sun *et al*., 2024), suggesting that CD44 genetic variations may affect disease progression and survival prognosis in CC patients. However, a study of 60 primary colon tumors showed that although CD44v was significantly more highly expressed in tumor tissues ($p < 0.0001$), its expression level was inversely associated with the risk of lymph node metastasis ($p = 0.040$) and distant metastasis ($p = 0.039$) and CD44v expression was further reduced in liver metastases ($p = 0.0005$) (Kaida *et al*., 2023) .This finding contrasts sharply with the positive correlation between CD44v6 and drug resistance observed in this study, further suggesting that CD44v function may be tumor-type- and disease-stage-specific. Future comparative studies are needed to explore this in depth.

The downstream signaling mechanisms by which miR-135 may inhibit CC cell proliferation and reverse cisplatin resistance by targeting CD44v6 remain to be elucidated. Previous studies have shown that in endometriosis, OPN splice variants activate the PI3K and NF-κB pathways by binding to CD44v, promoting cell proliferation, migration and EMT (Ho *et al*., 2022); in thyroid cancer, CD44 maintains cancer stem cell properties through the PI3K/Akt and Wnt/β-catenin pathways and promotes multidrug resistance by enhancing drug efflux via ABC transporters and evading apoptosis (Mosoane *et al*., 2025). Notably, members of the miR-135 family target distinct downstream genes across different tumors. In colorectal cancer, miR-135b targets SPOCK1 to regulate the Warburg effect and 5-fluorouracil resistance (Babaei-Jadidi *et al*., 2022); in breast cancer, miR-135 regulates proliferation and EMT through the Wnt/β-catenin signaling pathway (Jiang *et al*., 2022). These studies suggest that downregulation of miR-135 may upregulate CD44v6 and other target genes through derepression, activating the PI3K/AKT and Wnt/β-catenin pathways, enhancing cancer stem cell properties and anti-apoptotic capacity, thereby promoting cisplatin resistance. Relevant studies have confirmed that in colorectal cancer stem cells, CD44v6 activates the WNT/β-catenin pathway by forming a CD44v6-LRP6 signaling complex and upregulates MDR1 to mediate drug efflux, thereby promoting chemotherapy resistance (Ghatak *et al*., 2022b). This is similar to the results of this study. However, this study has not established a causal relationship. In the future, functional experiments are needed to determine whether CD44v6 is the key effector molecule mediating the chemotherapy-sensitization effect induced by miR-135.

Given the central regulatory role of miRNAs in tumorigenesis and drug resistance, miRNA-based therapy has emerged as a novel anticancer strategy. In this study, miR-135 was downregulated in drug-resistant cells and miR-135 mimic transfection reversed cisplatin resistance, suggesting that replenishing tumor-suppressive miRNAs has therapeutic potential. Currently, important progress has been made in the clinical translation of miRNA mimics and inhibitors. In breast cancer, PEGylated gold nanoparticles successfully delivered miR-206 to tumor cells, inducing apoptosis (Chaudhari *et al*., 2022). In clinical trials, LNA-i-miR-221 demonstrated excellent safety in patients with advanced refractory cancer, with 50% of patients achieving stable disease; the miR-155-targeting Cobomarsen has shown efficacy and tolerability in phase I/II trials in patients with lymphoma (Di Martino *et al*., 2025). These findings support the clinical feasibility of miRNA-based interventions. However, the clinical translation of miRNA therapies still faces challenges related to stability, targeted delivery and off-target effects. Delivery systems such as lipid nanoparticles and exosomes are being extensively studied. Future studies should validate the therapeutic efficacy and safety of miR-135 mimics in combination with cisplatin in animal models to facilitate clinical translation.

Although the roles of miR-135 in regulating chemoresistance and CD44v-associated drug resistance have been reported in other tumor models, the specific interaction between miR-135 and CD44v6 in cisplatin-resistant CC cells has not been previously described. Thus, this study is the first to identify the potential role of the miR-135–CD44v6 axis in reversing drug resistance in the HeLa/DDP model. However, this study has several limitations: only a single drug-resistant cell model (HeLa/DDP) was used and the results were not validated in cells of other genetic backgrounds; bioinformatic predictions were performed using only the TargetScan database and other CD44 variant isoforms were not evaluated for regulation by miR-135; a complete causal chain from miR-135 to CD44v6 to downstream signaling

pathways was not established; and *in-vivo* experiments and large-sample clinical validation are lacking. Future studies are needed to validate these findings through prospective studies, multiple cell models, and in *vivo* experiments.

CONCLUSION

Upregulation of miR-135 was associated with reduced CD44v6 expression, suppressed proliferation, increased apoptosis and enhanced cisplatin sensitivity in HeLa/DDP cells. These findings reveal an inverse association between miR-135 and CD44v6 in cisplatin-resistant CC cells; however, they do not establish a causal relationship. Future studies employing CD44v6-specific knockdown or rescue experiments are needed to determine whether CD44v6 directly mediates the chemosensitizing effects of miR-135.

Acknowledgments
We gratefully acknowledge the First Clinical Medical College of Guizhou University of Traditional Chinese Medicine Laboratory for providing the necessary equipment for this study.

Authors' contributions
Rui Zhou: Responsible for research design, experimental operation, data analysis, drawing verification and writing; Hongmei Wang: Data collation, drawing verification and experimental operation; Anji Li: Fund acquisition and project guidance; Shuhan Lv: Research conception and design, project management and supervision; All authors reviewed and approved the final version of the manuscript.

Funding
This work was supported by the National Natural Science Foundation of China Project (No. 82160851).

Data availability statement
All data generated or analyzed during this study are included in this published article and its supplementary information files.

Ethical approval
Since the datasets were from a cell experiment, ethics committee approval and patient consent were not required for this study and a clinical trial number is not applicable.

Conflict of interest
The authors declare no conflict of interest.

REFERENCES

Babaei-Jadidi R, Kashfi H, Alelwani W, Karimi Bakhtiari A, Kattan SW, Mansouri OA, Mukherjee A, Lobo DN and Nateri AS (2022). Anti-miR-135/SPOCK1 axis antagonizes the influence of metabolism on drug response in intestinal/colon tumour organoids. *Oncogenesis*., **11**(1): 4.

Bencheikh S, Lemriss H, Souiri A, Akachar J, Laarej K, Ameziane El Hassani R and Lemriss S (2026). Human papillomavirus-encoded microRNAs: Key regulators in cervical cancer development. *RNA Biol*., **23**(1): 1–14.

Cataldi-Stagetti E, Governatori G, Orsini A, De Nicolo B, Zagari RM and Bonora E (2026). MicroRNAs in esophageal cancer: Implications for diagnosis, progression, prognosis and chemoresistance. *Int J Mol Sci*., **27**(2): 878.

Chaudhari R, Nasra S, Meghani N and Kumar A (2022). MiR-206 conjugated gold nanoparticle based targeted therapy in breast cancer cells. *Sci Rep*., **12**(1): 4713.

Chen H, Ling R, Lai J, Liu Z, Wang Z, Yang H and Kong Y (2025). CD44v6-mediated regulation of gastric cancer stem cells: A potential therapeutic target. *Clin Exp Med*., **25**(1): 80.

Di Martino MT, Tagliaferri P and Tassone P (2025). MicroRNA in cancer therapy: Breakthroughs and challenges in early clinical applications. *J Exp Clin Cancer Res*., **44**(1): 126.

Di Y, Jiang Y, Shen X, Liu J, Gao Y, Cai H, Sun X, Ning D, Liu B, Lei J and Jin S (2021). Downregulation of miR-135b-5p suppresses progression of esophageal cancer and contributes to the effect of cisplatin. *Front Oncol*., **11**: 679348.

Ejima R, Suzuki H, Tanaka T, Asano T, Kaneko MK and Kato Y (2023). Development of a novel Anti-CD44 variant 6 monoclonal antibody C44Mab-9 for multiple applications against colorectal carcinomas. *Int J Mol Sci*., **24**(4): 4007.

Feitosa PSF, Fernandes FL, Pereira TP, Almeida DRQ, Carvalho AE, Almeida VD, Cavalcante GA, Júnior JADS, Rodrigues TD, Nascimento EGCD, Bezerra CM, Fernandes JV and Fernandes TAAM (2024). Alterations in miRNA expression and their role in the pathogenesis of cervical cancer. *Asian Pac J Cancer Prev*., **25**(10): 3533–3541.

Ghatak S, Hascall VC, Karamanos N, Markwald RR and Misra S (2022a). Interplay between chemotherapy-activated cancer associated fibroblasts and cancer initiating cells expressing CD44v6 promotes colon cancer resistance. *Front Oncol*., **12**: 906415.

Ghatak S, Hascall VC, Karamanos N, Markwald RR and Misra S (2022b). Chemotherapy induces feedback up-regulation of CD44v6 in colorectal cancer initiating cells through β-catenin/MDR1 signaling to sustain chemoresistance. *Front Oncol*., **12**: 906260.

Gong Y, Xiong Y, Gao Y, Song X, Gong Y, Wang D, Liu Z, Yang Y, Lu J, Zou IX and Shi X (2025). Verteporfin inhibits the cGAS-STING pathway and improves the tumor microenvironment during cisplatin treatment in hepatocellular carcinoma. *Front Immunol*., **16**:

1658042.

Hirayama A, Tanaka T, Ohishi T, Shinoda K, Nakamura T, Nomura A, Kojo N, Araki H, Suzuki K, Kaneko MK, Suzuki H and Kato Y (2025). Therapeutic potential of an anti-CD44v6 monoclonal antibody in xenograft models of colorectal and gastric cancer. *Cells*., **14**(23): 1873.

Ho NT, Lin SW, Lee YR, Tzeng CR and Kao SH (2022). Osteopontin splicing isoforms contribute to endometriotic proliferation, migration and epithelial-mesenchymal transition in endometrial epithelial cells. *Int J Mol Sci*., **23**(23): 15328.

Jiang D, Zhou B, Xiong Y and Cai H (2022). [Corrigendum] miR-135 regulated breast cancer proliferation and epithelial-mesenchymal transition acts by the Wnt/β-catenin signaling pathway. *Int J Mol Med*., **50**(2): 105.

Julianti RA, Putra AD, Fuady A, Nuranna L, Purwoto G, Nuryanto KH and Yudhistira MY (2026). Expression of miR-92a and miR-125b and their association with chemoradiotherapy response in locally advanced cervical cancer. *Int J Mol Sci*., **27**(4): 1723.

Kadkhoda S, Eslami S, Mahmud Hussen B and Ghafouri-Fard S (2022). A review on the importance of miRNA-135 in human diseases. *Front Genet*., **13**: 973585.

Kaida T, Fujiyama Y, Soeno T, Yokota M, Nakamoto S, Goto T, Watanabe A, Okuno K, Nie Y, Fujino S and Yokota K (2023). Less demand on stem cell marker-positive cancer cells may characterize metastasis of colon cancer. *PLoS One*., **18**(4): e0277395.

Kundu M, Butti R, Panda VK, Malhotra D, Das S, Mitra T, Kapse P, Gosavi SW and Kundu GC (2024). Modulation of the tumor microenvironment and mechanism of immunotherapy-based drug resistance in breast cancer. *Mol Cancer*., **23**(1): 92.

Lee C, Kim MJ, Kumar A, Lee HW, Yang Y and Kim Y (2025). Vascular endothelial growth factor signaling in health and disease: From molecular mechanisms to therapeutic perspectives. *Signal Transduct Target Ther*., **10**(1): 170.

Liu P, Zhu Y, Zhou H and Li R (2025). Trends and urban-rural disparities in cervical cancer epidemiology in China, *Sci Rep*., **15**(1): 25021.

Lodewijk I, Duenas M, Paramio JM and Rubio C (2023). CD44v6, STn and O-GD2: Promising tumor associated antigens paving the way for new targeted cancer therapies. *Front Immunol*., **14**: 1272681.

Mosoane B, McCabe M, Jackson BS and Dlamini Z (2025). CD44 variant expression in follicular cell-derived thyroid cancers: Implications for overcoming multidrug resistance. *Molecules*., **30**(9): 1899.

Park MN, Kim M, Lee S, Kang S, Ahn CH, Tallei TE, Kim W and Kim B (2025). Targeting redox signaling through exosomal MicroRNA: insights into tumor microenvironment and precision oncology. *Antioxidants (Basel)*, **14**(5): 501.

Peng F, Fan H, Li S, Peng C and Pan X (2021). MicroRNAs in epithelial-mesenchymal transition process of cancer: Potential targets for chemotherapy. *Int J Mol Sci*., **22**(14): 7526.

Queffeulou M, Fakhfakh R, Fani F, Dos Santos A, Reis Ferreira G, Bigot S, Godin C, Leprohon P, Papadopoulou B and Ouellette M (2025). CRISPR-Cas13b mediated gene knockdowns in Leishmania infantum. *Int J Parasitol Drugs Drug Resist*., **29**: 100629.

Raftery MJ, Franzen AS, Radecke C, Boulifa A, Schönrich G, Stintzing S, Blohmer JU and Pecher G (2023). Next generation CD44v6-Specific CAR-NK cells effective against triple negative breast cancer. *Int J Mol Sci*., **24**(10): 9038.

Shiri Aghbash P, Hemmat N, Baradaran B and Bannazadeh Baghi H (2023). siRNA-E6 sensitizes HPV-16-related cervical cancer through Oxaliplatin: An *in-vitro* study on anti-cancer combination therapy. *Eur J Med Res*., **28**(1): 42.

Srikanth A, Rao RVA, Dong R, Tharehalli U, Barth TFE, Dembowsky K, Seufferlein T, Schirmbeck R and Lechel A (2025). Peptide-based inhibition of CD44v6 renders liver carcinomas more susceptible to therapeutic intervention. *J Mol Med (Berl)*., **103**(11-12): 1583–1598.

Sun YH, Wang CM, Shen HP, Lee CY, Lin CW, Yang SF and Wang PH (2024). Impact of CD44 genetic variants on clinicopathological characteristics of uterine cervical cancer patients. *Int J Med Sci*., **21**(8): 1428–1437.

Suwiwat S, Tungsinmunlong K and Siriaungkul S (2022). Expression of CD44v6 and RCAS1 in uterine cervical carcinoma infected with human papillomavirus and its effect on cell proliferation and differentiation. *Asian Pac J Cancer Prev*., **23**(7): 2431–2439.

Tao W, Wang W, Zhai J and Guo L (2023). Efficacy analysis of neoadjuvant versus adjuvant cisplatin-paclitaxel regimens for initial treatment of FIGO stages IB3 and IIA2 cervical cancer. *Med Sci Monit*., **29**: e940545.

Wilczyński JR, Szubert M, Paradowska E and Wilczyński M (2022). Endometriosis stem cells as a possible main target for carcinogenesis of endometriosis-associated ovarian cancer (EAOC). *Cancers (Basel)*., **15**(1): 111.

Wise AR, Maloney S, Hering A, Zabala S, Richmond GE, VanKlompenberg MK, Nair MT and Prosperi JR (2024). Bcl-2 Up-regulation mediates taxane resistance downstream of APC Loss. *Int J Mol Sci*., **25**(12): 6745.

Zhang G, Lan H, Wu J, Sheng X, Huang L, Zhou M and Hu J (2025). Ganoderic acid a potentiates cisplatin's cytotoxicity on gallbladder cancer cells by promoting DNA damage and inhibiting cell stemness. *World J Surg Oncol*., **23**(1): 148.

Zhang H, Zhou Z, Wang J, Wang S, Ren J, Zhang M and Yang M (2025). Adverse drug reaction assessment of pembrolizumab in cervical cancer treatment: A real-world pharmacovigilance study using the FAERS database. *Front Immunol*., **16**: 1582050.

Zhao L, Zhai Q, Zhang W, Wen L, Fu X, Xie X, Jin X, Zhang N, Meng Y, Li L and Gu C (2026). Favorable short-term survival in locally advanced cervical cancer with optimal pathological response after neoadjuvant chemoimmunotherapy: A real-world analysis. *Front Immunol*., **17**: 1737081.

Zhou Z, Zhong H, Wang H, Wang S, Kridis WB, Wang R, Shen K, Wang Z and Huang R (2025). Microenvironmental regulation and remodeling of breast cancer angiogenesis: From basic mechanisms to clinical therapeutic implications. *Discov Oncol*., **16**(1): 1973.